NASA
Technical
Paper
2139

May 1983

Morphology of an Aluminum Alloy Eroded by a Jet of Angular Particles Impinging at Normal Incidence

P. Veerabhadra Rao,
Stanley G. Young,
and Donald H. Buckley

NASA
Technical
Paper
2139

1983

Morphology of an Aluminum Alloy Eroded by a Jet of Angular Particles Impinging at Normal Incidence

P. Veerabhadra Rao
Lewis Research Center
Cleveland, Ohio

Stanley G. Young
Kennedy Space Center
Kennedy Space Center, Florida

Donald H. Buckley
Lewis Research Center
Cleveland, Ohio

NASA
National Aeronautics
and Space Administration

**Scientific and Technical
Information Branch**

Summary

A morphological study of the erosion of an aluminum alloy by normal impact of crushed glass erodent particles has been conducted. Erosion patterns were studied at several stages of erosion by varying driving-gas pressure and exposure time. The surfaces were studied with scanning electron microscopy and energy dispersive X-ray spectroscopy. A profilometer was used to measure surface profiles. Transformation from deformation to cutting wear induced by the erosion process was observed, and the dynamics of the erosion is discussed herein.

The morphology of the damage pattern reflects the flow of erodent particles inside the pit. From morphologic comparisons of the pits over driving-gas pressures from 0.14 to 0.82 MPa, and after exposure times from 2.5 to 10 minutes, damage mechanisms were postulated and further insight into the erosion process was gained. Four distinct erosion regions were identified: region 1, at the center of the pit, consists of irregular surfaces; region 2, on the side slope of a pit, consists of small but clear concentric ripples; region 3, a rough transition zone at pit edge; and region 4 varies from incipient erosion to a completely undamaged zone. The concentric ripples of region 2 appeared after a certain time had elapsed and once the pit had reached a width-to-depth ratio of around 2. Cutting wear predominated at advanced stages in all of the erosion zones. Evidence for deformation wear appeared at the initial stages of erosion. The transformation to cutting wear phenomenon appeared to occur simultaneously as the erosion rate transformed the incubation period to the acceleration period. The embedment of crushed glass was maximum at the bottom of the pit and decreased gradually from the pit edge to the undamaged region.

Introduction

Erosion of ductile materials by solid particle impingement has been studied for several years as a result of detrimental effects of erosion in practical applications, including turbomachinery, tactical military aircraft, helicopters, etc. (e.g., refs. 1 to 3). Many investigators (refs. 4 to 32) have studied different aspects of erosion with particle impact in order to gain understanding the fundamental mechanisms of the erosion processes. However, in actual erosion situations the particles are considerably smaller and more angular than those used in the spherical particle impingement studies.

An erosion model suggested by Finnie (ref. 5) in 1958 has related solid particle impingement erosion of ductile materials to a micromachining process. Bitter (ref. 6) suggested that total erosion of different materials at any angle of incidence may be divided into cutting wear and deformation wear. The latter predominates at normal incidence, which was attributed to work-hardening and embrittlement. The elaborate analysis of Bitter was simplified by Neilson and Gilchrist (ref. 8) to better represent the experimental data. Tilly (ref. 9) has discussed the erosion of ductile materials as a two-stage process consisting of the primary impact and secondary fragmentation effects, with subsequent outflow. Other mechanisms suggested for material removal are extrusion, delamination of subsurface layers, melting, low cycle fatigue, adiabatic shear localization, adhesive material transfer, etc. Unfortunately, a single mechanism cannot fully account for the total material damage with all shapes of impinging particles. It is generally observed that two or three mechanisms contribute to total cumulative erosion (e.g., refs. 3, 20, 30, and 31).

Parametric studies pertaining to different abrasives and other details, such as distance, nozzles, etc., were reported by many investigators (e.g., refs. 4, 11 to 13, and 32). It has been observed that angular particles cause more erosion than spherical particles. Weight gains were also reported to be due to the embedment of angular particles during the initial phases of erosion (refs. 14, 16, and 19). The particle mean size of less than 5 μm was able to cause negligible erosion except in a few real situations (ref. 11).

A recent study using angular particles postulated the mechanism of material removal as an extrusion process ending in ductile fracture with possible low-cycle fatigue or delamination wear (ref. 31). However, the flake type structure observed on materials eroded by spherical particles (refs. 26, 27, and 29) has not been observed on materials eroded by angular particles. The micrographs presented by different investigators show cutting type mechanisms for materials eroded by angular particles. Recently, plowing and two types of cutting mechanisms with single particles were studied in detail (ref. 30).

Despite the many studies (refs. 4 to 32) conducted so far, the fundamental understandinng of the morphology on the surfaces of materials after erosion and a generalized theory to predict erosion resistance are not yet available. Little attention has been given to the erosion process and wear mechanisms for angular particles with respect to erosion time. The objective of this present study was to determine the morphology of erosion damage resulting from impacting angular particles of crushed glass at various pressures and exposure times. The effect of exposure time on erosion and a transition of the wear mechanism from deformation to cutting are also discussed. Surface chemistry analyses were made to determine the interaction of erodent particles and target metal and to determine the extent of embedment of crushed glass particles into the surface.

Experimental Facility and Test Conditions

The investigations reported in this paper were conducted with a commercial sandblaster. A schematic of the nozzle arrangement is shown in figure 1. Samples of ductile metals were eroded at normal incidence with high-velocity, commercial grade 10 crushed glass particles of 30-μm mean size. (A scanning electron micrograph of crushed glass particles was presented in ref. 24.) Argon was used as the driving gas to minimize possible chemical influences on target metal surfaces. The driving-gas pressure was varied from 0.14 to 0.82 MPa (gage). Because of the complexity of flow and particle size variations within the jet, no attempt was made to measure the impingement velocities; however, the jet velocity at the center of the nozzle exit is assumed to be 75 to 80 m/sec at a driving-gas pressure of 0.31 MPa (ref. 33). The distance between the specimen and the nozzle (1.18 mm diam) was 13 mm.

The aluminum alloy 6061-T6511 was chosen for this study because it is commonly used in structures and is a well characterized alloy. The composition and mechanical properties of this alloy are given in reference 34. The alloy was solution heat-treated and artificially aged. Before exposure to crushed-glass impingement, all specimens were polished with 600-grit emery paper, then with 3-μm diamond paste and were cleaned with distilled water.

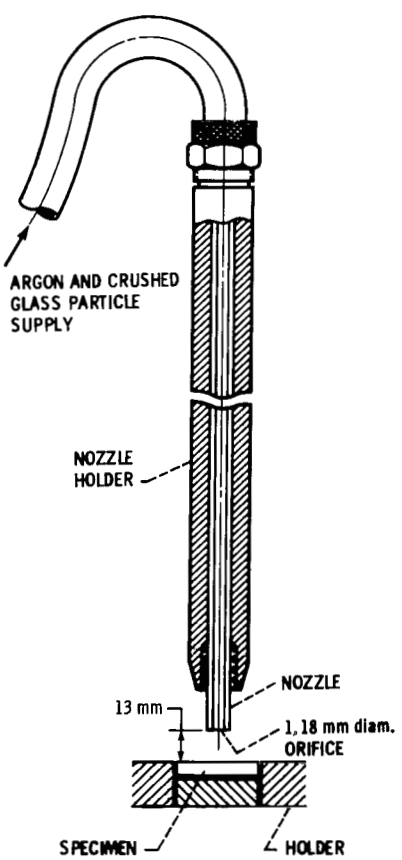

Figure 1. - Schematic diagram of nozzle holder arrangement for steady-jet impingement.

The crushed glass particles were passed through the nozzle only once. The weight loss values of the eroded specimens were determined after each exposure to the jet of crushed glass. The surfaces were blown with compressed air to clean them of loose glass particles. The surfaces were then measured with a profilometer, were observed with a scanning electron microscope (SEM), and were analyzed for chemical composition using energy dispersive X-ray spectroscopy (EDS).

Results and Discussion

Description of the Erosion Pattern

Figure 2 shows scanning electron micrographs of an aluminum alloy specimen exposed to crushed glass impingement for 10 minutes at 0.54 MPa driving-gas pressure. Figure 3 is a surface profile of the same specimen. The specimen, photographed at an advanced stage of erosion, shows an erosion pattern that reveals four distinct regions.

Region 1, at the pit bottom, consists mainly of irregular surfaces (no clear cut pattern). Region 2, on the slopes of the pit, consists of concentric ripple patterns. The surface profile (fig. 3) shows that the slope is very steep and that the rings consist of very small steps (less than 20 μm) with rounded edges inside the pit. Region 3 is not as steep as region 2 and consists of a transition slope from horizontal to the pit edge. This region is rougher than the other regions, with undulations varying from 2 to 5 μm. Region 4 consists of a transition from the completely undamaged zone to the incipient erosion zone. Surface disturbance is observed in this region in the form of random cuts and scratches.

Figure 4 is a series of scanning electron micrographs of aluminum alloy specimens tested at six pressures, 0.14, 0.27, 0.41, 0.54, 0.68, and 0.82 MPa, and at four exposure times, 2.5, 5, 7.5, and 10 min. The driving-gas pressure increases from top to bottom, and time increases from left to right. Specimens of the earliest stages of erosion do not show ripple patterns. The inception of ripple formation in region 2 can be seen in figures 4(j), (m), (q), and (u).

Table I presents pit widths, depths, and width to depth ratios for aluminum alloy specimens impacted with crushed glass at different presssures and times. The widths or average diameters are measured from the surface traces recorded on all the specimens. A close observation of figure 4 and the results in table I indicate that ripples initiate when the ratio of width to depth is around 2.5. As this ratio approaches 2, the ripples have fully developed.

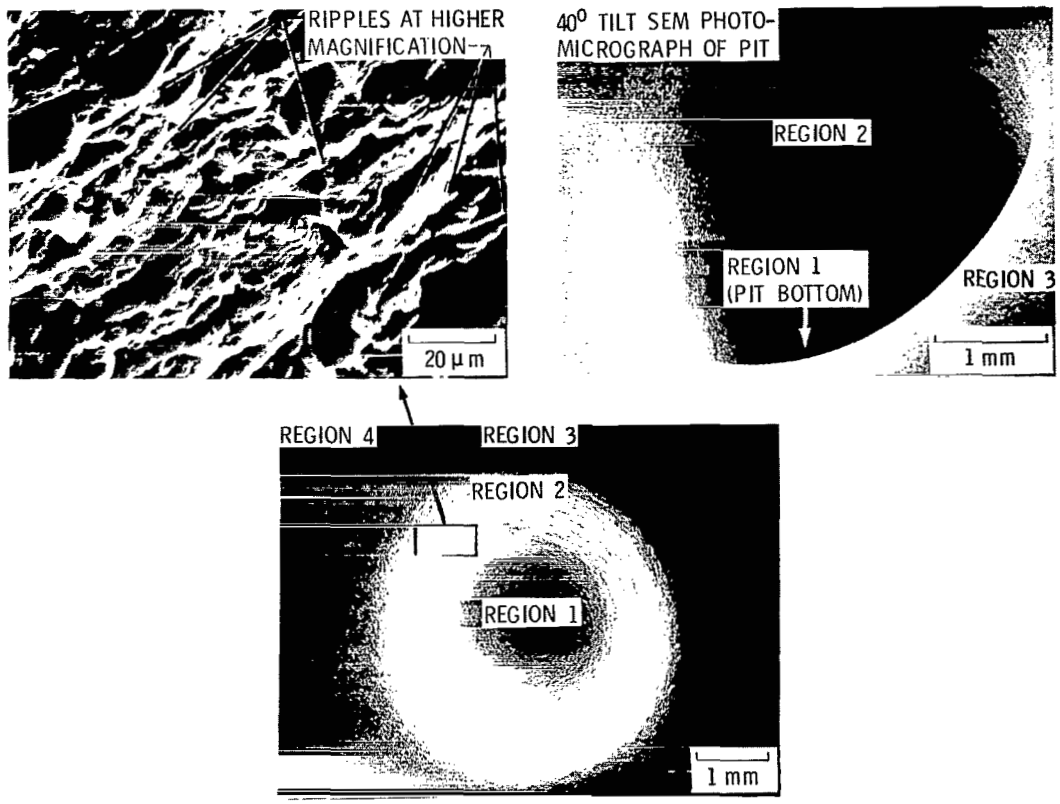

Figure 2. - Scanning electron micrographs of eroded aluminum alloy surface after exposure to crushed-glass-particle impingement. Driving-gas pressure, 0.54 MPa; exposure time, 10 min.

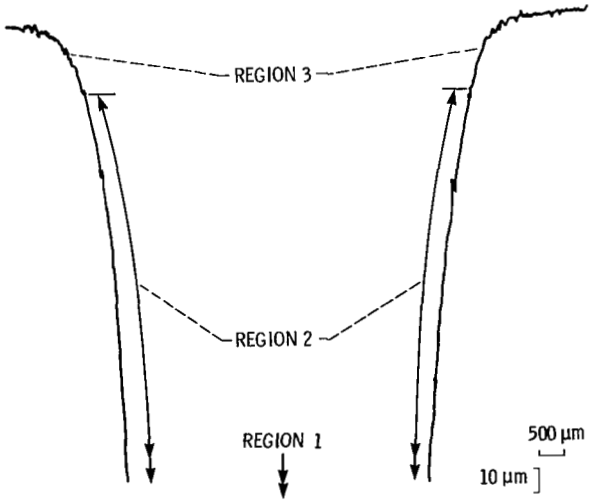

Figure 3. - Surface profile of eroded aluminum alloy surface after exposure to crushed-glass-particle impingement. Driving-gas pressure, 0.54 MPa; exposure time, 10 min.

TABLE I. - WIDTHS AND DEPTHS OF PITS AND THEIR RATIOS FOR ALUMINUM ALLOY SPECIMENS EXPOSED TO CRUSHED GLASS IMPINGEMENT

[Pit width measurements were made from surface traces.]

Exposure time, min	Parameter of pit	Gas pressure of jet, MPa (gage)					
		0.14	0.27	0.41	0.54	0.68	0.82
2.5	Width, w, μm	3780	4070	5690	6450	6300	6520
	Depth, d, μm	132	914	1608	1836	2413	2449
	w/d	28.6	4.45	3.54	3.51	2.61	2.66
5.0	Width, w, μm	3800	5700	6500	6850	6700	6630
	Depth, d, μm	152	1412	2565	3228	3541	3919
	w/d	25.0	4.04	2.53	2.12	1.89	1.69
7.5	Width, w, μm	3850	5930	6570	6950	6930	6850
	Depth, d, μm	180	1841	3162	3820	4542	4826
	w/d	15.2	3.22	2.08	1.82	1.53	1.42
10.0	Width, w, μm	4040	6200	6670	6950	7040	7000
	Depth, d, μm	254	1991	3414	4610	4948	5095
	w/d	15.9	3.11	1.95	1.51	1.42	1.34

The results presented in table I further indicate that both width and depth of pits increase but that their growth rates decrease with both time and pressure. The depth increases faster than the width, which accounts for the decreasing rates as time and pressure increase.

Some investigators (refs. 4, 7, 10, 12, 22, 27, and 35) described a regular spaced ripple pattern with hills and valleys at low angle of incidence using both angular and spherical particles. The ripples on the pit sides in this investigation are very irregular. Moore (ref. 36) obtained almost perfect right-angled steps on 90° conical targets. He has, however, attributed this step type ripple

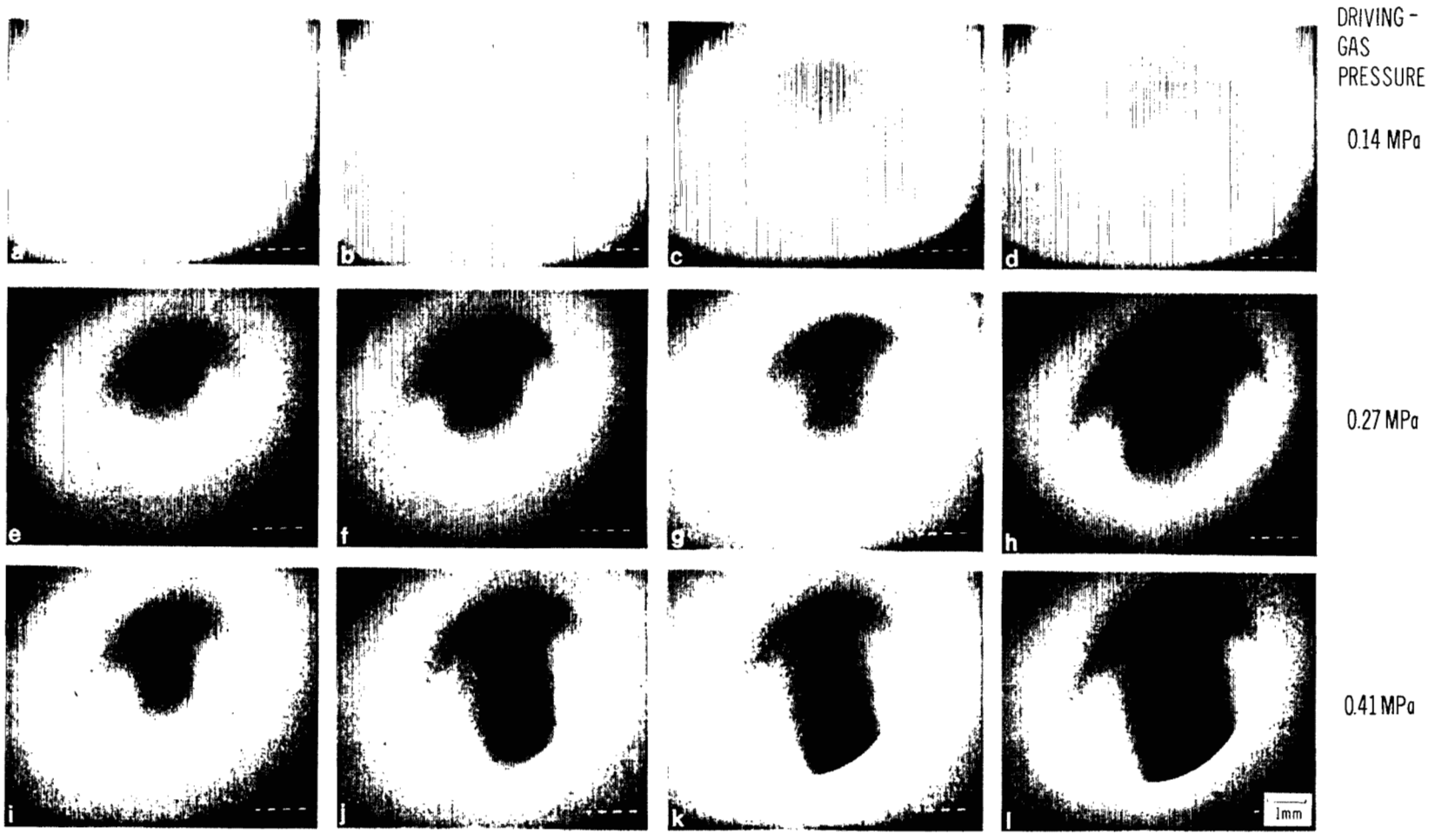

Figure 4. - Scanning electron micrographs (40° tilt) of eroded aluminum alloy surfaces after exposure to crushed-glass impingement.

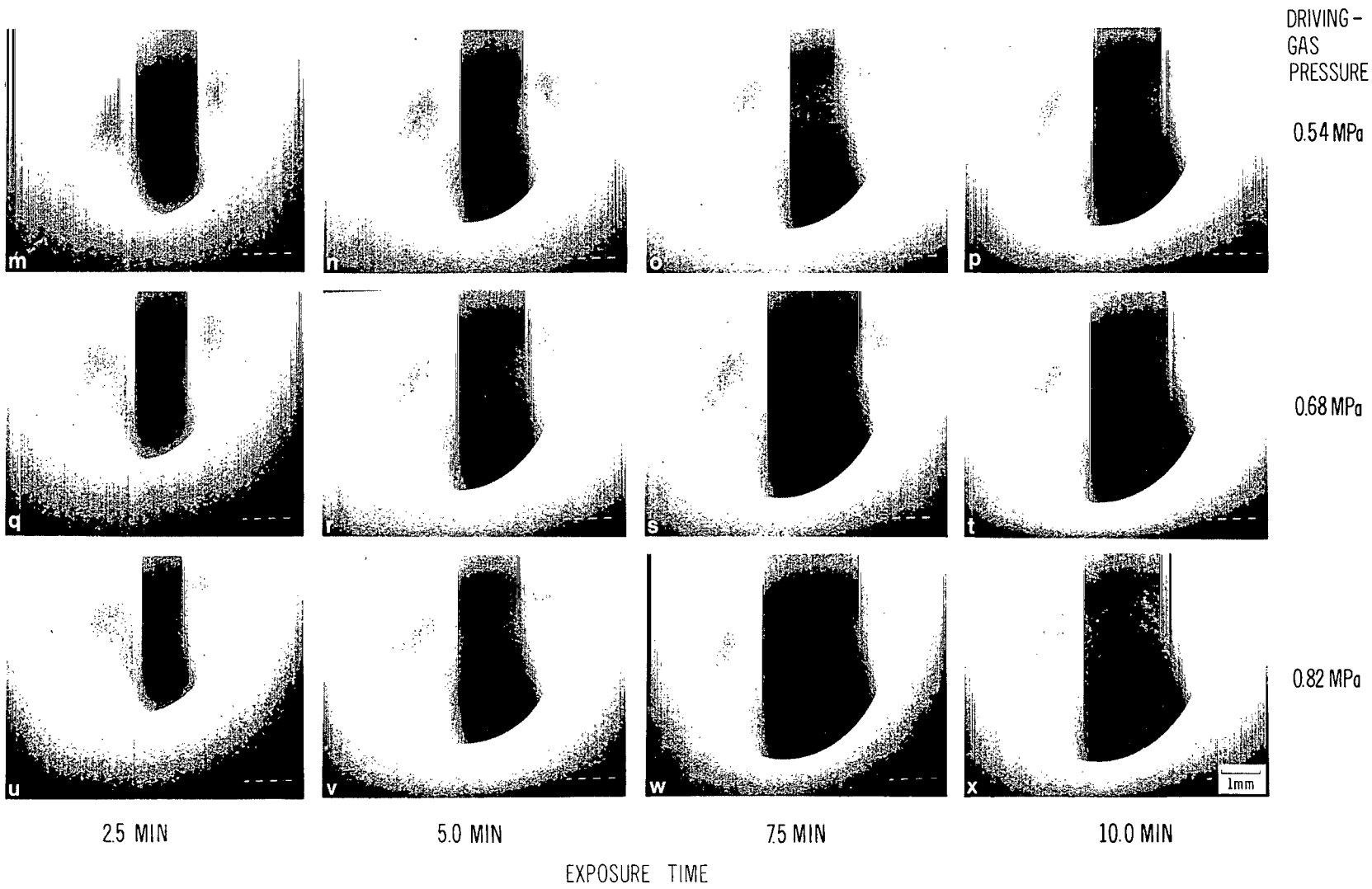

Figure 4. - Concluded.

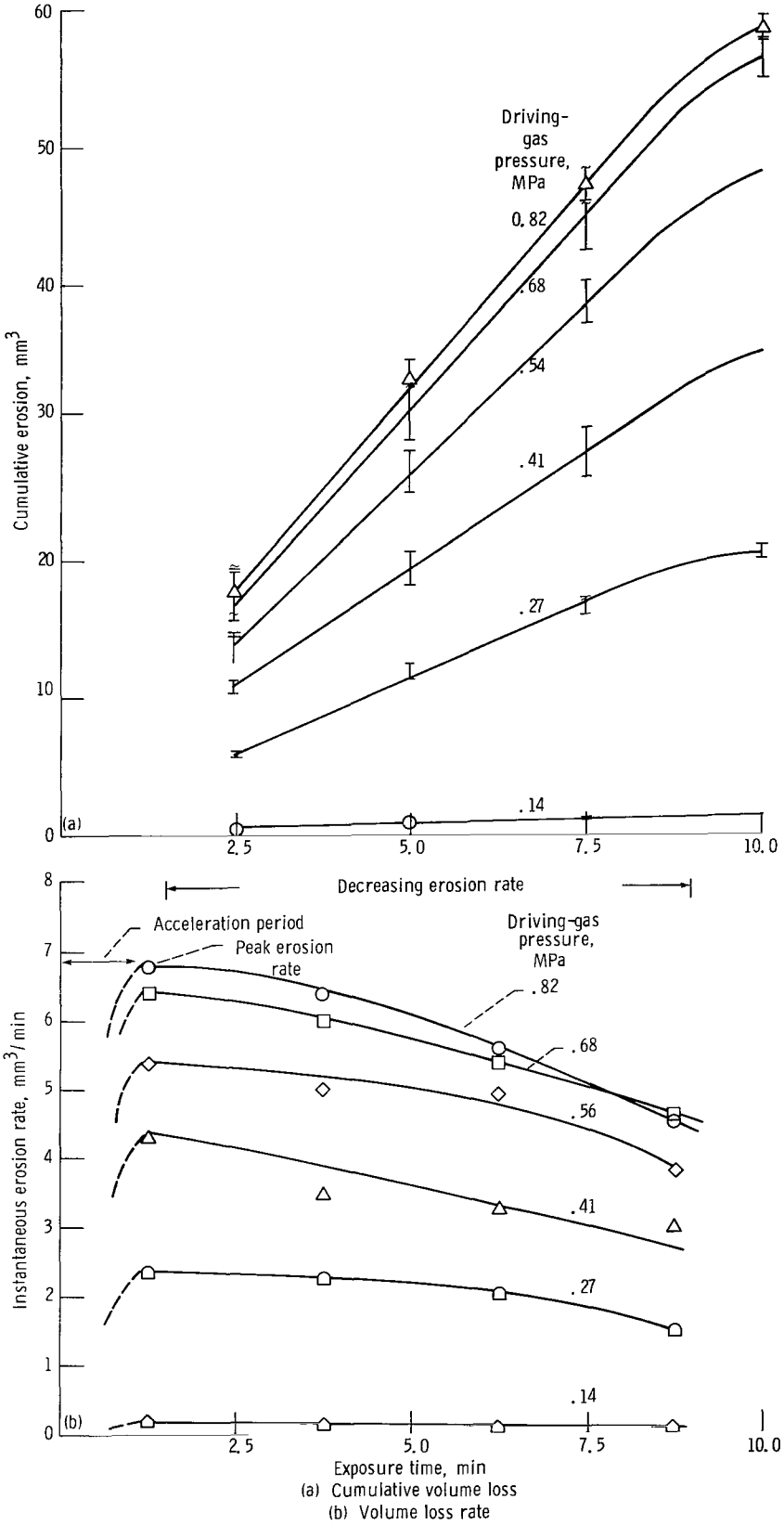

Figure 5. - Erosion versus time curves.

formation to plastic flow progress before thin flakes of metal are detached. Finnie and Kabil (ref. 10) were able to explain the regular ripple pattern that forms when ductile materials are eroded at angles which correspond with maximum volume loss. Their theoretical explanation of this phenomenon at low angles of incidence (15° to 35°) is as follows: An impacted surface resulting in irregularities may be described as forming an infinite series of sinusoidal waves whose amplitudes and phases are functions of a specific wavelength, which depends on material properties and dynamic particle interaction conditions. They argued further that there should be a wavelength for which wave growth rate is maximum and that this particular wavelength will eventually appear as a ripple pattern. As erosion continues, the ripples of this optimum wavelength will grow in amplitude and that eventually the radius of curvature of valleys will decrease to the size of the eroding particles. Hence, further growth of ripples of this wavelength will not be possible, and ripples of longer wavelengths will occur. By this mechanism peaks will be attacked less severely than valleys, so that irregularities would tend to grow further.

This mechanism is believed to be pertinent to ripple formation found in the present study for the following reason. The angle of impingement changes from normal to nearly glancing as the pit deepens with exposure time. Ripples did not form initially when the flat surface was eroded with crushed glass, but as the pit deepened. Ripple formation appeared to form when jet and pit configuration reach a low angle of incidence (~15° to 35°) corresponding to maximum volume loss. The irregular and gradually decreasing size ripple patterns of this study may partially be attributed to interference between oncoming and outgoing (rebounding) particles in the erosion pit. This type of suggestion was also made by Moore (ref. 36). The present study shows that impact pressure plays a critical role on the rate of development of the damage patterns.

The ripple formation is not seen in figures 4(a) to (i) because the advanced erosion stages have not been reached at either the shortest time or lowest gas pressures.

Effect of Time on Erosion

Figure 5 presents cumulative erosion-time and instantaneous erosion-rate-time curves for the aluminum alloy exposed to crushed glass impingement. Table II presents the cumulative volume loss data for the different pressures and exposure times. Mean (and standard deviation) values shown in table II are plotted in figure 5(a) and, in general, demonstrate good reproducibility. Exposure times corresponding with the patterns observed in figure 4 may be compared on the curves of figure 5(a). Erosion-rate-time curves in figure 5(b) indicate an acceleration period (time span during which the erosion rate increases rapidly to peak value), peak erosion rate and a continuously decreasing erosion rate period (deceleration period). These differ from most reported erosion-rate-time curves, which indicate an initial acceleration period and a final steady-state period (e.g., refs. 14, 16, and 37).

Both widening and deepening of the pits (table I) appear to contribute to the acceleration period, peak rate, and deceleration period. The rates of deepening and widening also roughly show the same trends as those

TABLE II. - EXPERIMENTAL DATA FOR ALUMINUM ALLOY SPECIMENS IMPACTED WITH CRUSHED MICRO-GLASS PARTICLE IMPINGEMENT

[Calibrated crushed glass average flow rates, 4.8, 20.1, 21.1, 15.3, 13.3 and 12.9 g/min at 0.14, 0.27, 0.41, 0.54, 0.68 and 0.82 MPa (gage) driving gas pressures, respectively.]

Pressure, MPa (gage)	Time, min	Number of specimens tested	Average volume loss, mm^3	Standard deviation
0.14	2.5	5	0.49	0.25
	5.0	4	.87	.11
	7.5	3	1.11	.11
	10.0	2	1.38	NA[a]
0.27	2.5	5	5.88	0.20
	5.0	4	11.55	.73
	7.5	3	16.65	.68
	10.0	2	20.43	NA
0.41	2.5	5	10.82	0.29
	5.0	4	19.56	1.12
	7.5	3	27.72	1.66
	10.0	2	35.20	NA
0.54	2.5	5	13.59	1.17
	5.0	4	26.08	1.37
	7.5	3	38.45	1.61
	10.0	2	48.01	NA
0.68	2.5	5	16.30	1.56
	5.0	4	31.28	1.97
	7.5	3	44.71	2.07
	10.0	2	56.35	NA
0.82	2.5	5	17.06	1.16
	5.0	4	33.05	.98
	7.5	3	47.06	1.04
	10.0	2	58.45	NA

[a]Not applicable.

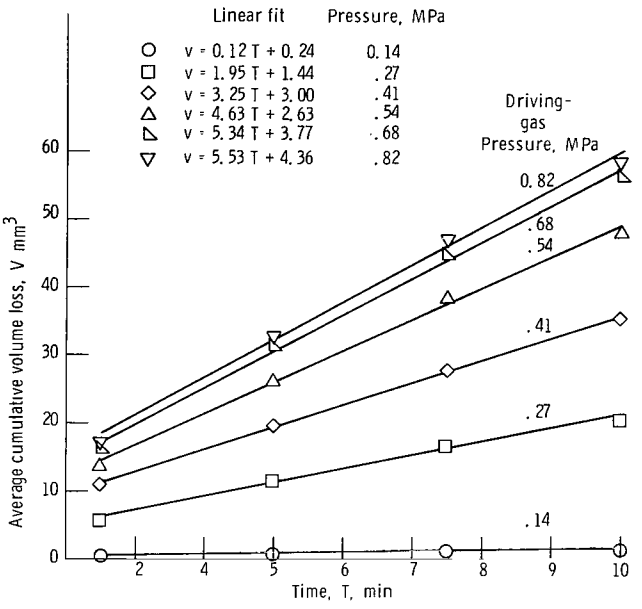

Figure 6. - Cumulative erosion as function of time for impingement of crushed glass on aluminum alloy.

shown in figure 5(b). The present studies indicate that as the ratio decreases, the erosion rate also decreases. Further study is necessary, however, to understand more about the erosion rate-time curves under different experimental conditions.

Experiments conducted for very short exposure times during the initial phases of erosion (up to 1 min) indicated weight gains of a few hundredths of a milligram only. Other investigators (refs. 8, 14, 16, 19, and 37), however, observed a considerable deposition or embedment of angular particles contributing to considerable weight gains. The almost negligible amount of deposition noted in the present study may be attributed to low impact pressures, small particle sizes, and low concentrations of crushed glass.

Figure 6 shows the same data as plotted in figure 5(a); however, least-squares linear fits are projected through the data and equations for the curves at each pressure condition are shown. The primary conclusion from these data is that there appears to be an upper limit to the damage rate at a pressure above 0.7 MPa (probably related to the nozzle diameter).

The following is a discussion of how the pit morphology changes with exposure time.

A set of surface profiles of the aluminum alloy specimen tested at the lowest pressure, 0.14 MPa, is shown in figure 7. The exposure times of 2.5, 5, 7.5, and 10 minutes correspond with photographs in figure 4(a) to (d), respectively. For this specimen no measurable weight loss was recorded up to the 30 to 45 seconds of exposure, although the surface traces indicate a small depressed area. After 45 seconds, volume loss was evident. With the exception of 0.14 MPa driving-gas pressure, it appears that by 2.5-minute exposure all specimens attained peak erosion-rate conditions (fig. 5(b)).

Figures 8 and 9 present higher magnification scanning electron micrographs of regions 2 and 3 for 0.14, 0.27, and 0.54 MPa. A comparison of figures 4, 8, and 9 indicates the changes took place in each region with respect to exposure time as well as driving-gas pressure. Both regions 1 and 2 increased in area with respect to time. Figure 8 shows arc-type rippled patterns with spongy appearance except at 0.14 MPa. Figure 9 exhibits jagged, angular craters and cut surfaces with chips, characteristic of cutting wear (refs. 30 and 31), except at 0.14 MPa pressure. In both cases a transition of the surface from dented to jagged was observed (see fig. 10). It is therefore believed that there is a transition of the wear mechanism from deformation to cutting (ref. 30), which may correspond to the change from incubation to accelerated damage. We surmise that, initially, a well-contoured pit induces outflow of particles of angular material at the edges, which causes cutting on the surface as particles break off. Hence, the surface morphology may contribute to cutting induced by direct impact and outflow. In these experiments cutting induced by direct impact seemed to be less than that induced by outflow.

Influence of Flow Velocity

The impingement velocity is one of the most important influences on erosion. Recent studies (refs. 2, 3, 21, 30

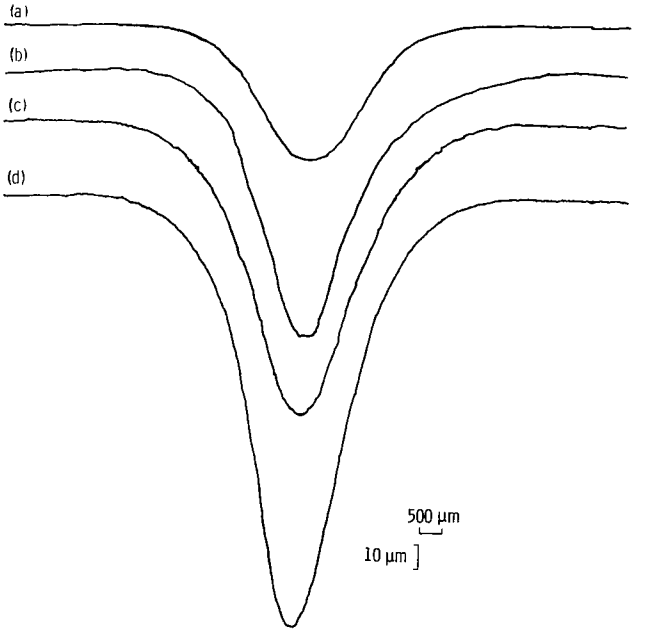

(a) Time, 2.5 minutes
(b) Time, 5.0 minutes
(c) Time, 7.5 minutes
(d) Time, 10.0 minutes

Figure 7. - Surface profiles of aluminum alloy specimen after exposure to crushed-glass-particle impingement. Driving gas pressure, 0.14 MPa.

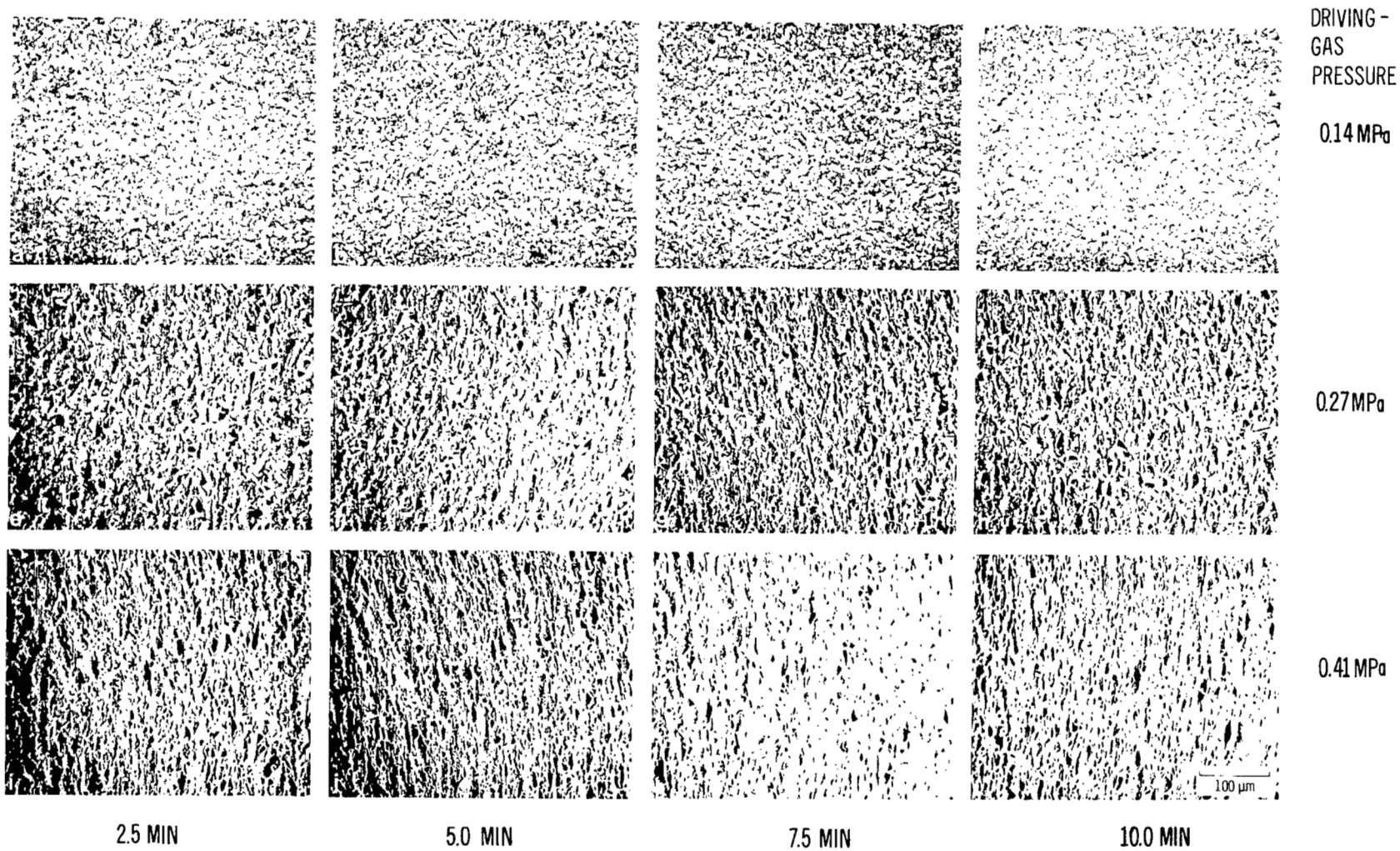

Figure 8. - Scanning electron micrographs of eroded aluminum alloy surfaces after exposure to crushed-glass-particle impingement. Region 2.

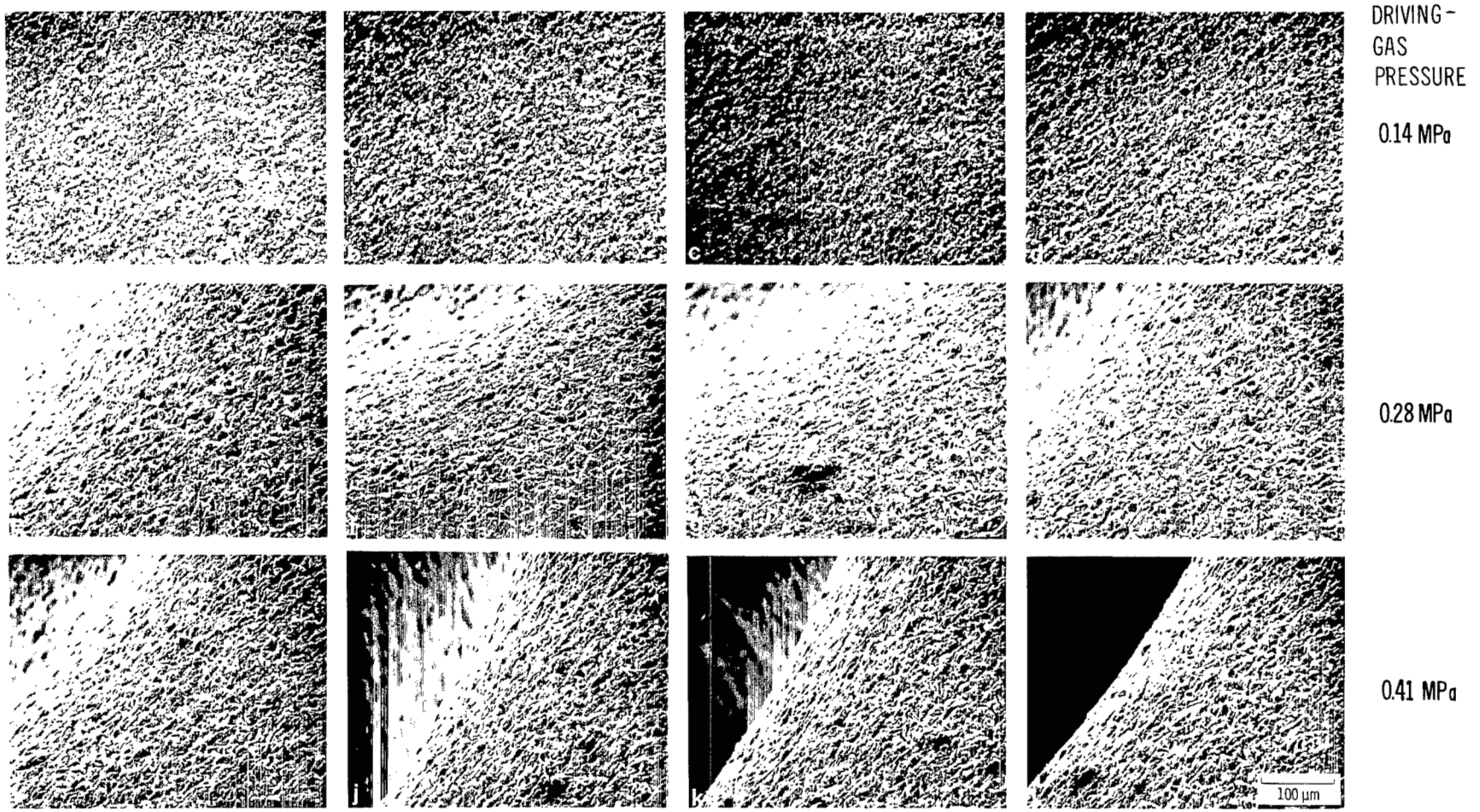

Figure 9. - Scanning electron micrographs (40° tilt) of eroded aluminum alloy surfaces after exposure to crushed-glass-particle impingement. Region 3.

and 31), using different experimental conditions and both spherical and angular particles, show a wide variation in the correlation of erosion rate with velocity. The reported velocity exponents did not agree well with each other, even at normal incidence (refs. 21 and 30). A detailed discussion of some of these discrepancies has been made by Hutchings (ref. 30) and Finnie, et al. (ref. 31).

The free-stream velocity of a jet at any instant follows a relationship that velocity is proportional to the square root of pressure. The mean erosion rates (slopes of linear equations in fig. 6) have been converted to cubic millimeters per gram of crushed glass using calibrated crushed-glass particle flow rates (table II). All values of free-stream velocities and erosion rates have been normalized with respect to the quantities used at 0.41 MPa pressure. The crushed-glass flow rate is maximum ($\sim$0.35 g/sec) at this pressure. The least square fit of these normalized data (fig. 11) results in a velocity exponent of 3.25.

Figure 11 also presents data on aluminum collected from the literature (refs. 8 and 38) other than data analyzed in reference 26. The present value of 3.25 and a value of 3.15 for the data of Neilson and Gilchrist (ref. 8) are in close agreement with the velocity exponents (3 to 3.4) reported earlier for normal incidence (ref. 26). The data in reference 38 are surprisingly consistent with both plots. However, individual least-square analysis of data in reference 38 results in exponents of 1.1 to 1.4 due to very large particles (400 μm) and a whirling arm experimental device. It has to be realized that the good consistency obtained in figure 11 is most encouraging despite the many differences in data-taking equipment and procedures. Figure 11 further indicates that particles up to 200-μm may not influence the exponential relation. Angular particles of 400 μm size, however, affect the power law relation between the erosion rate and velocity and considerably decrease the velocity exponent. It is further believed that the high values of exponents found in figure 11 may possibly be the result of aerodynamic effects discussed by Laitone (refs. 39 and 40) for normal impingement.

Surface Chemistry Analysis

After exposure to erosion, EDS analyses were made at the bottom and edge of the pit and on the aluminum alloy surface far away from the pit (fig, 12). The silicon peak indicates the presence of glass. The bottom of the pit (fig. 12(a)) contains more glass than the edge of the pit (fig. 12(b)), and very little (if any) glass is observed far away from the pit (fig. 12(c)). It is believed that fine, broken crushed glass particles are embedded or trapped in the rough surface. However, within the sensitivity of the EDS used in this study, none were observed within the pit. A few isolated particles of glass were observed outside the pit.

The concept of an embedded (or even fused) erodent particle layer on the surface (refs. 14, 16, and 19) seems to be possible. The amount of silicon appeared to be relatively constant across the pit bottom, with a continuous tapering off as distance from the pit edge increased.

Further studies and other analytic techniques are necessary to determine the (a) exact chemical nature of the tested sample surface, (b) embedment of particles and their influence on the erosion process at all stages, (c) material removal processes, and (d) fracture mechanisms of the erodent particles and material surfaces.

Summary of Results

Impact erosion experiments using crushed glass particles at normal incidence have been conducted on an aluminum alloy at six driving-gas pressures and for four exposure times. Changes in surface morphology and the

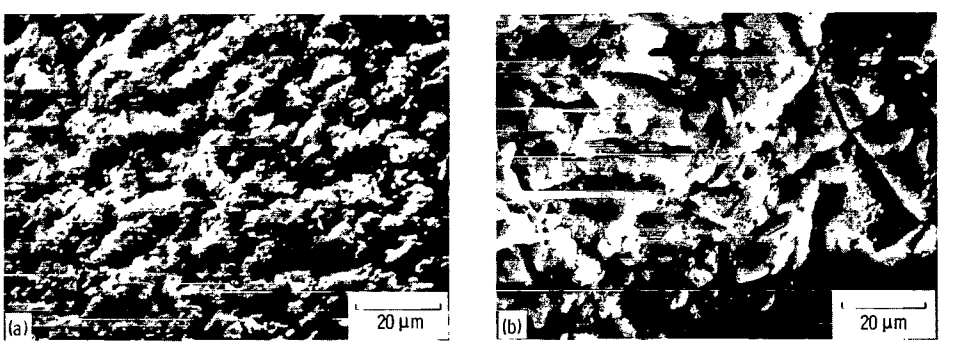

(a) Driving-gas pressure, 0.14 MPa; exposure time, 2.5 min.
(b) Driving-gas pressure, 0.54 MPa; exposure time, 10 min.

Figure 10. - Scanning electron micrographs (40° tilt) of an eroded aluminum alloy surface after exposure to crushed-glass-particle impingement. Region 3.

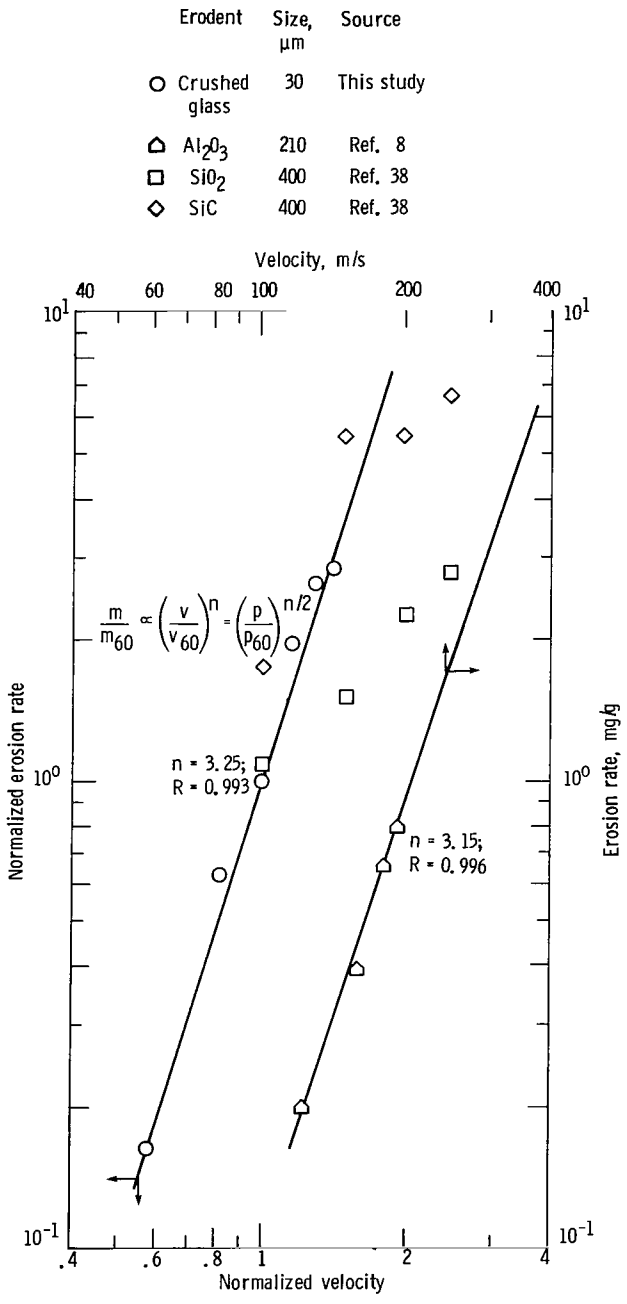

Figure 11. - Variation of erosion rate with velocity. R denotes correlation coefficient for the curves.

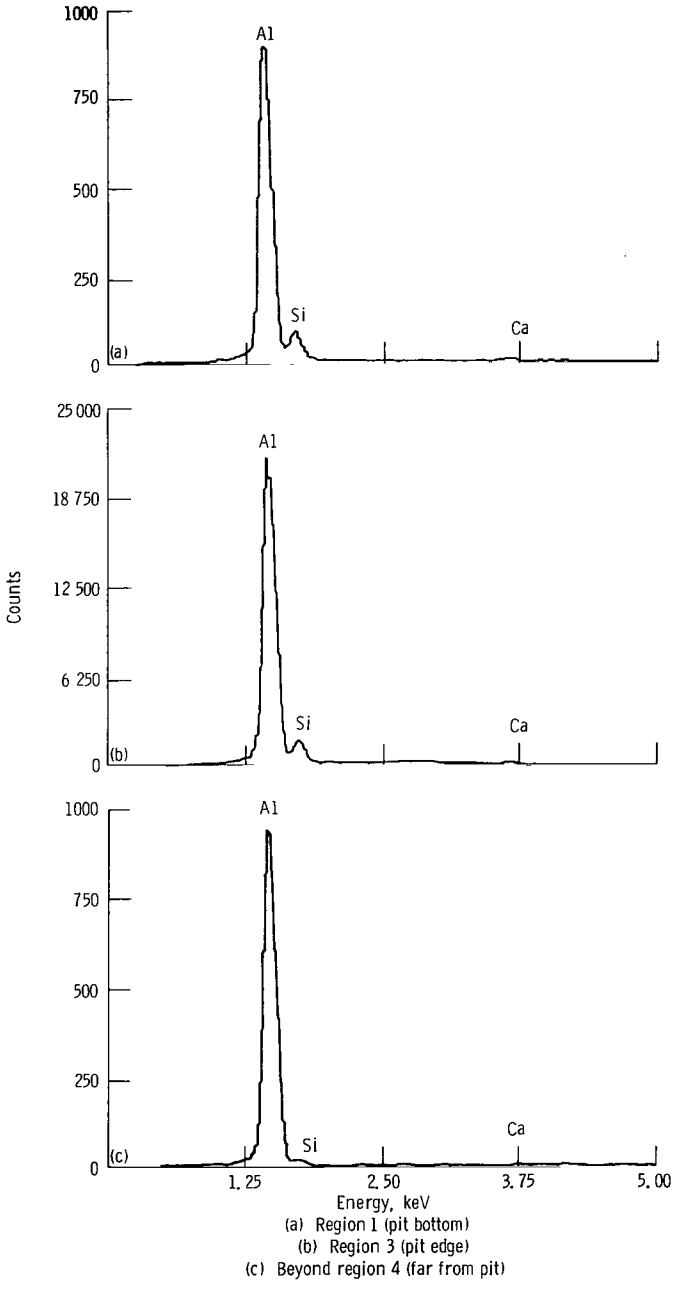

Figure 12. - EDS analysis of aluminum specimen surface showing silicon peaks, indicating the presence of trapped crushed glass on the surface.

relationships of these changes to the erosion process were studied.

Four regions in the erosion pattern can be identified: region 1, at the center of the pit or impact, consisting of irregular surfaces; region 2, consisting of small but clear concentric ripples within the side slope of a pit; region 3, a rough transition zone with a varying slope from horizontal to almost vertical at pit edge; and region 4, which varies from completely undamaged to incipient erosion. Both regions 1 and 2 increase in size and area with exposure time and attain a saturated maximum for a given driving-gas pressure. The ripple formation in region 2 is attributed to the outflow of crushed glass once the pit reaches a width to depth ratio of pits around 2.

Erosion-rate-time curves indicate an acceleration period, a peak, and a gradually decreasing rate of erosion.

As the driving-gas pressure increases, the erosion rate increases, and morphological transformation of the eroded pits occurs earlier.

During the inception of damage, a transition from deformation wear to cutting wear appears; however, as

erosion develops, cutting wear appears to dominate, and the removal process accelerates.

The embedment of crushed glass particles is maximum and relatively uniform at the pit bottom and decreases gradually from the edge of the pit to the undamaged metal.

Lewis Research Center
National Aeronautics and Space Administration
Cleveland, Ohio, November 12, 1982

References

1. Hibbert, W. A.: Helicopter Trials Over Sand and Sea. J. Roy. Aeronaut. Soc., vol. 69, no. 659, Nov. 1965, pp. 769-776.
2. Adler, W. F.: Assessment of the State of Knowledge Pertaining to Solid Particle Erosion. Rept. ETI CR 79-680, Contract DAAG 29-77-C-0039, U.S. Army Research Office, 1979.
3. Schmitt, G. F., Jr.: Liquid and Solid Particle Impact Erosion. Wear Control Handbook, M. P. Peterson and W. O. Winer, eds., American Society of Mechanical Engineers, 1980, pp. 231-282.
4. Russel, A. S.; and Lewis, J. E.: Abrasive Characteristics of Alumina Particles. Ind. Eng. Chem., vol. 46, 1954, pp. 1305-1310.
5. Finnie, I.: The Mechanism of Erosion of Ductile Metals. Proceedings, Third National Congress of Applied Mechanics, American Society of Mechanical Engineers, 1958, pp. 527-532.
6. Finnie, I.: Erosion of Surfaces by Solid Particles. Wear, vol. 3, 1960, pp. 87-103.
7. Bitter, J. G. A.: A Study of Erosion Phenomena—Part I and Part II. Wear, vol. 6, 1963, pp. 5-21 and 169-190.
8. Neilson, J. H.; and Gilchrist, A.: Erosion by a Stream of Solid Particles. Wear, vol. 11, 1968, pp. 111-121.
9. Tilly, G. P.: A Two-Stage Mechanism of Ductile Erosion. Wear, vol. 23, 1973, pp. 87-96.
10. Finnie, I.; and Kabil, Y.H.: On the Formation of Surface Ripples During Erosion. Wear, vol. 8, 1965, pp. 60-69.
11. Tilly, G. P.; and Sage, W.: The Interaction of Particle and Material Behavior in Erosion Processes. Wear, vol. 16, 1970, pp. 447-465.
12. Smeltzer, C. E.: Gulden, M. E.; and Compton, W. A.: Mechanisms of Metal Removal by Impacting Dust Particles. J. Basic Eng., vol. 92, no. 3, 1970, pp. 639-654.
13. Young, J. P.; and Ruff, A. W.: Particle Erosion Measurements on Metals. J. Eng. Mater. Technol., vol. 99, no. 2, Apr. 1977, pp. 121-125.
14. Kosel, T. H.; Turner, A. P. L.; and Scattergood, R. O.: Effects of Particle Size and Shape on Erosive Wear Mechanisms. Corrosion-Erosion Behavior of Materials, K. Natesan, ed., The Metallurgical Society of AIME, 1978, pp. 146-161.
15. Ruff, A. W.: Debris Analysis of Erosive and Abrasive Wear. Fundamentals of Tribology, 1978, N. P. Suh and N. Saka, eds., MIT Press, 1980, pp. 877-885.
16. Kosel, T. H.; Scattergood, R. O.; and Turner, A. P. L.: An Electron Microscope Study of Erosive Wear. Wear of Materials 1979, K. C. Ludema, W. A. Glaeser and S. K. Rhee, eds., American Society of Mechanical Engineers, 1979, pp. 192-204.
17. Christman, T.; and Shewmon, P. G.: Adiabatic Shear Localization and Erosion of Strong Aluminum Alloys. Wear, vol. 54, no. 1, 1979, pp. 145-155.
18. Finnie, I.: Some Observations on the Erosion of Ductile Metals. Wear, vol. 19, 1972, pp. 81-90.
19. Ives, L. K.; and Ruff, A. W.: Electron Microscope Study of Erosion Damage in Copper. Erosion: Prevention and Useful Applications, W. F. Adler, ed., Am. Soc. Test. Mater. Spec. Tech. Publ. (664), 1977, pp. 5-35.
20. Brainard, W. A.; and Salik, J.: Scanning Electron-Microscope Study of Normal-Impingement Erosion of Ductile Metals. NASA TP-1609, 1980.
21. Rickerby, D. G.; and Macmillan, N. H.: The Erosion of Aluminum by Solid Particle Impingement at Normal Incidence. Wear, vol. 60, no. 2, 1980, pp. 369-382.
22. Carter, G.; Nobes, M. J.; and Arshak, K. I.: The Mechanism of Ripple Generation on Sandblasted Ductile Solids. Wear, vol. 65, 1980, pp. 151-174.
23. Salik, J.; Buckley, D. H.; and Brainard, W. A.: The Effect of Mechanical Surface and Heat Treatments on the Erosion Resistance of 6061 Aluminum Alloy. Wear, vol. 65, no. 3, 1981, pp. 351-358.
24. Salik, J.; and Buckley, D. H.: Effect of Erodent Particle Shape and Various Heat Treatments on Erosion Resistance of Plain Carbon Steel. NASA TP-1755, 1981.
25. Bellman, R.: and Levy, A. V.: Platelet Mechanism of Erosion of Ductile Metals. Wear of Materials 1981. S. K. Rhee, A. W. Ruff and K. C. Ludema, eds., American Society of Mechanical Engineers, 1981, pp. 564-576.
26. Hutchings, I. M.: A Model for the Erosion of Metals by Spherical Particles at Normal Incidence. Wear, vol. 70, no. 3, 1981, pp. 269-281.
27. Brown, R.; Jun, E. J.; and Edington, J. W.: Erosion of α-Fe by Spherical Glass Particles. Wear, vol. 70, no. 3, 1981, pp. 347-363.
28. Brown, R.; and Edington, J. W.: The Melting of Metal Targets During Erosion by Hard Particles. Wear, vol. 71, no. 1, Sept. 1981, pp. 113-118.
29. Rao, Veerabhadra P.; Young, S. G.; and Buckley, D. H.: Morphology of Ductile Metals Eroded by a Jet of Spherical Particles Impinging at Normal Incidence. Wear, vol. 85, no. 2, 1983, pp. 223-237.
30. Hutchings, I. M.: Mechanisms of the Erosion of Metals by Solid Particles. Erosion: Prevention and Useful Applications, W. F. Adler, ed., ASTM STP-664, American Society for Testing and Materials, 1977, pp. 59-76.
31. Finnie, I.; Levy, A.; and McFadden, D. H.: Fundamental Mechanisms of the Erosive Wear of Ductile Metals by Solid Particles. Erosion: Prevention and Useful Applications, W. F. Adler, ed., ASTM STP-664, American Society for Testing and Materials, 1977, pp. 36-58.
32. Wolak, J.; et al.: Parameters Affecting the Velocity of Particles in an Abrasive Jet. J. Eng. Mater. Technol., vol. 99, no. 2, Apr. 1977, pp. 147-152.
33. Ruff, A. W.; and Ives, L. K.: Measurement of Solid Particle Velocity in Erosive Wear. Wear, vol. 35, 1975, pp. 195-199.
34. Sheldon, G. L.; and Finnie, I.: On the Ductile Behavior of Nominally Brittle Materials During Erosive Cutting. J. Eng. Ind., vol. 88, no. 4, Nov. 1966, pp. 387-392.
35. Duffin, H. C.: A Laboratory Scale Study of Erosion and Deposition Due to Gas Borne Solids. National Gas Turbine Establishment Memorandum No. M.341, Aug. 1960.
36. Moore, M. B.: Mechanisms of Erosion of Ductile Metals by Solid Impingement. NYO-3477-12, Rutgers Univ., Mar. 1968.
37. Soderberg, S.; et al.: Erosion Classification of Materials Using a Centrifugal Erosion Tester. Tribol. Int., vol. 14, no. 6, Dec. 1981, pp. 333-343.
38. Kayser, W.: Erosion by Solid Bodies. Proc. 2nd Meerburg Conference on Rain Erosion and Allied Phenomena, A. A. Fyall and R. B. King, eds., Royal Aircraft Establishment, Farnborough, 1967, pp. 427-447.
39. Laitone, J. A.: Aerodynamic Effects in the Erosion Process. Wear, vol. 56, no. 1, Sept. 1979, pp. 239-246.
40. Laitone, J. A.: Erosion Prediction Near a Stagnation Point Resulting from Aerodynamically Entrained Solid Particles. J. Aircraft, vol. 16, no. 12, Dec. 1979, pp. 809-814.

1. Report No.	2. Government Accession No.	3. Recipient's Catalog No.
NASA TP-2139		

4. Title and Subtitle
MORPHOLOGY OF AN ALUMINUM ALLOY ERODED BY A JET OF ANGULAR PARTICLES IMPINGING AT NORMAL INCIDENCE

5. Report Date
May 1983

6. Performing Organization Code
506-53-12

7. Author(s)
P. Veerabhadra Rao, Stanley G. Young, and Donald H. Buckley

8. Performing Organization Report No.
E-1166

10. Work Unit No.

9. Performing Organization Name and Address
National Aeronautics and Space Administration
Lewis Research Center
Cleveland, Ohio 44135

11. Contract or Grant No.

13. Type of Report and Period Covered
Technical Paper

12. Sponsoring Agency Name and Address
National Aeronautics and Space Administration
Washington, D. C. 20546

14. Sponsoring Agency Code

15. Supplementary Notes
P. Veerabhadra Rao, National Research Council - NASA Research Associate; Stanley G. Young, Kennedy Space Center, Florida; and Donald H. Buckley, Lewis Research Center.

16. Abstract
The erosion of an aluminum alloy impinged by crushed glass particles at normal incidence was studied. The erosion patterns were analyzed by scanning electron microscopy, energy dispersive X-ray spectroscopy, and surface profilometer measurements. From the analysis of specimens tested at various driving gas pressures and time intervals, four distinct erosion regions were identified. A study of pit morphology and its relationship to cumulative erosion was made. Cutting wear is believed to be the predominant material removal mechanism; some evidence of deformation wear was found during the incubation period.

17. Key Words (Suggested by Author(s))
Morphology; Erosion; Aluminum alloy; Particle impingement; Jet impact

18. Distribution Statement
Unclassified - unlimited
STAR Category 26

19. Security Classif. (of this report)	20. Security Classif. (of this page)	21. No. of Pages	22. Price*
Unclassified	Unclassified	15	A02

* For sale by the National Technical Information Service, Springfield, Virginia 22161

NASA-Langley, 1983

1 1 1U,C, 830509 S00903DS
DEPT OF THE AIR FORCE
AF WEAPONS LABORATORY
ATTN: TECHNICAL LIBRARY (SUL)
KIRTLAND AFB NM 87117